HHS Public Access

Author manuscript

JACC Basic Transl Sci. Author manuscript; available in PMC 2018 March 06.

Published in final edited form as:

JACC Basic Transl Sci. 2017 October ; 2(5): 543–560. doi:10.1016/j.jacbts.2017.03.016.

Cardiosphere-Derived Cells Demonstrate Metabolic Flexibility That Is Influenced by Adhesion Status

Junaid Afzal, MBBS, MS[a,b], **Angel Chan, MD, PhD**[a], **Mehmet Fatih Karakas, MD**[a], **Kirubel Woldemichael, BS**[a], **Styliani Vakrou, MD**[a], **Yufan Guan, MD**[a], **Jeffrey Rathmell, PhD**[c], **Richard Wahl, MD**[d], **Martin Pomper, MD, PhD**[e], **D. Brian Foster, PhD**[a], **Miguel A. Aon, PhD**[a,f], **Benjamin Tsui, PhD**[e], **Brian O'Rourke, PhD**[a], and **M. Roselle Abraham, MD**[a,b]

[a]Department of Medicine, Johns Hopkins School of Medicine, Baltimore, Maryland [b]Division of Cardiology, University of California San Francisco, San Francisco, California [c]Department of Pathology, Microbiology and Immunology, Vanderbilt University Medical Center, Nashville, Tennessee [d]Department of Radiology, Washington University School of Medicine, St. Louis, Missouri [e]Department of Radiology, Johns Hopkins School of Medicine, Baltimore, Maryland [f]National Institute on Aging/National Institutes of Health, Baltimore, Maryland

SUMMARY

Adult stem cells demonstrate metabolic flexibility that is regulated by cell adhesion status. The authors demonstrate that adherent cells primarily utilize glycolysis, whereas suspended cells rely on oxidative phosphorylation for their ATP needs. Akt phosphorylation transduces adhesion-mediated regulation of energy metabolism, by regulating translocation of glucose transporters (GLUT1) to the cell membrane and thus, cellular glucose uptake and glycolysis. Cell dissociation, a pre-requisite for cell transplantation, leads to energetic stress, which is mediated by Akt dephosphorylation, downregulation of glucose uptake, and glycolysis. They designed hydrogels that promote rapid cell adhesion of encapsulated cells, Akt phosphorylation, restore glycolysis, and cellular ATP levels.

Graphical abstract

ADDRESS FOR CORRESPONDENCE: Dr. M. Roselle Abraham, UCSF Division of Cardiology, 555 Mission Bay Boulevard South, Smith Cardiovascular Research Building, 352G, San Francisco, California 94143. Roselle.Abraham@ucsf.edu.

All authors attest they are in compliance with human studies committees and animal welfare regulations of the authors' institutions and Food and Drug Administration guidelines, including patient consent where appropriate. For more information, visit the *JACC: Basic to Translational Science* author instructions page.

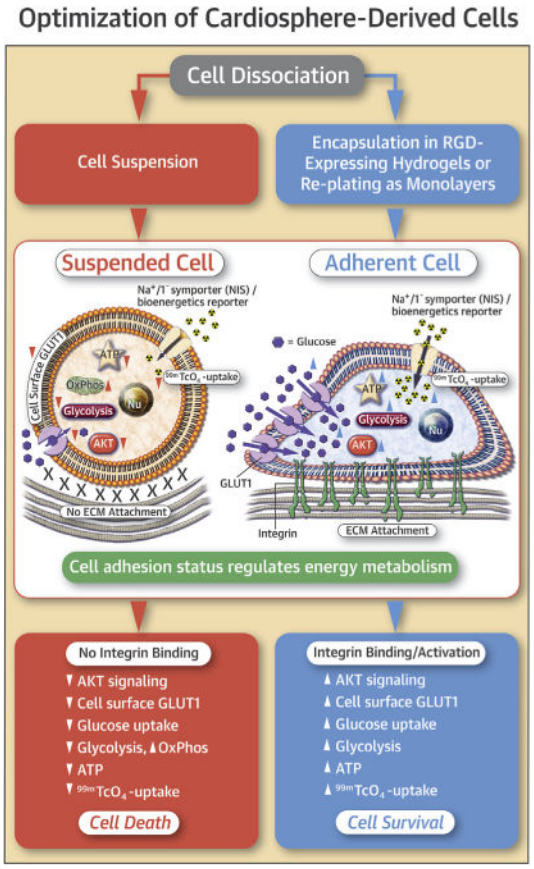

Afzal, J. et al. J Am Coll Cardiol Basic Trans Science. 2017;2(5):543-60.

Keywords

cardiosphere-derived cells (CDCs); glycolysis; metabolism; oxidative phosphorylation (OxPhos); sodium-iodide symporter (NIS); SPECT imaging

Cellular cardiomyoplasty is limited by low levels of transplanted cell engraftment (1). One possible contributor to low engraftment is the need for cell dissociation/suspension, which leads to down-regulation of metabolism, and anoikis (2,3). Yet, very little is known about the mechanisms underlying the metabolic effects of cell suspension and whether strategies that improve energy metabolism of suspended cells might increase their viability. Studies in adherent stem/progenitor cells reveal high rates of glucose metabolism via glycolysis (4) to generate lactate, despite oxygen availability, which is referred to as aerobic glycolysis or the Warburg effect (5). Although the ATP yield of glycolysis is lower than oxidative phosphorylation (OxPhos), glycolysis supplies metabolic intermediates for biosynthetic processes (e.g., nucleotide, amino acid, and lipidogenesis), which is advantageous for rapidly proliferating cells (5). High rates of glucose metabolism can also inhibit the pyruvate dehydrogenase complex, leading to inhibition of OxPhos (also called the Crabtree effect) (6) and shunting of pyruvate into lactate. But, it has not yet been determined if cell viability can

be increased by switching glycolysis to OxPhos (which is more efficient at ATP generation) during conditions of energetic stress such as cell dissociation/suspension (2,3).

In this study, we performed a detailed investigation of metabolism in suspended and adherent cells cultured as monolayers (2-dimensional [2D]) or encapsulated in hydrogels (3-dimensional [3D]), with the goal of identifying metabolic strategies that acutely improve the energetics and viability of suspended cells. Most of the studies were performed using rat cardiosphere-derived cells (CDCs) (7), which are currently in phase 2 clinical trials (ALLSTAR [ALLogeneic Heart STem Cells to Achieve Myocardial Regeneration], DYNAMIC [Dilated cardiomYopathy iNtervention with Allogeneic MyocardIally-regenerative Cells), to promote cardiac regeneration (8–10); targeted metabolic studies were also performed in human adipocyte stromal cells (11,12). We discovered that proliferating CDCs possess metabolic flexibility, and cell attachment status modulates cellular energetics dynamically. CDCs adherent for ≥3 h rely primarily on glycolysis for ATP generation and possess the ability to up-regulate glycolysis/glycolytic ATP generation following inhibition of OxPhos—we refer to this phenomenon as *glycolytic reserve* (13–16). In contrast, suspended CDCs down-regulate glucose uptake/glycolysis and have an increased reliance on OxPhos for ATP generation. Energetic stress and viability of suspended CDCs was improved by stimulation of OxPhos using pyruvate or serum, but cellular ATP levels were still lower than in adherent cells, suggesting the importance of cell adhesion in restoration of energetics. We designed scaffolds (HA:Bl:Ser hydrogels) that provide adhesion motifs (17–19) to encapsulated cells, and demonstrate that cell encapsulation in hydrogels stimulates integrin activation, ATP generation by OxPhos/glycolysis, rapid restoration of cellular ATP levels, and cell viability in vitro. In vivo energetic restoration in transplanted CDCs was confirmed by single-photon emission computed tomography (SPECT) imaging in the rat model following transplantation of CDCs expressing the Na^+-iodide symporter (NIS) (3,20). NIS actively cotransports Na^+ and the radiotracer ^{99m}Tc-pertechnetate into cells, using the electrochemical Na^+ gradient generated by Na^+/K^+-ATPase (21). We demonstrate that intracellular ^{99m}Tc-pertechnetate transport by NIS mirrors cellular ATP levels using in vitro metabolic restriction and metabolic inhibitors, and in vivo by SPECT imaging. NIS^+CDC encapsulation in hydrogels resulted in high cell-derived ^{99m}Tc-pertechnetate uptake (SPECT signal) within 3 h of transplantation, whereas reversible Akt inhibition, which transiently reduces cellular ATP levels, led to low ^{99m}Tc-pertechnetate uptake at this time point. Taken together, our studies indicate the presence of energetic stress in suspended cells that can be improved by stimulation of OxPhos using substrates or scaffolds that activate cell adhesion.

METHODS

MATERIALS

Stock solutions of oligomycin (oligo), FCCP (carbonyl cyanide-4-trifluoromethoxyphenyl-hydrazone), rotenone, antimycin A, and PI3K-Akt inhibitors were prepared in dimethyl sulfoxide. All compounds were diluted (1:5,000) prior to treatment. Iodoacetate (iodo) stock solution was prepared in water, and a final concentration of 1:500 was used. All control conditions were treated with vehicle (dimethyl sulfoxide or water) using the same concentration as the treatment condition.

CELL CULTURE

CDC isolation—Briefly, small pieces of heart tissue (explants) derived from male 10-week-old Wistar Kyoto (WK) rats were placed on fibronectin-coated dishes, as described previously (8,22). In the following days, cells exited the explants and formed an adherent monolayer with phase-bright cells on the top. These cells were harvested by mild enzymatic digestion and transferred to D-poly-lysine coated dishes, where they form 3D structures called cardiospheres that are enriched in cardiac progenitors (20). Cardiospheres were subsequently harvested and grown as monolayers in fibronectin-coated flasks—these cells are called CDCs. CDCs were cultured in IMDM medium (Catalog #15-016-CV, Corning, Edison, New Jersey) containing 10% fetal bovine serum (FBS), 2 mmol/l glutamine, and 0.1 mmol/l β-mercaptoethanol, and expanded to 3 to 5 passages prior to experiments.

Human adipocyte stromal cells (Catalog #R7788115 Thermo Fisher, Waltham, Massachusetts) were cultured in Dulbecco's Modified Eagle's Medium (DMEM) (Catalog #10-013, Corning) containing 10% FBS as previously described (12). Human bone marrow–derived mesenchymal stem cells (Catalog #A15652, Thermo Fisher) were cultured in STEMPRO mesenchymal stem cell (MSC) SFM medium obtained from Thermo Fisher. Neonatal rat ventricular myocytes (NRVMs) were isolated from 2-day-old neonatal rat pups, as previously described (23).

PREPARATION OF CELL SUSPENSIONS

For suspension culture, 10 × PolyHema solution was prepared by dissolving 1.2 g of PolyHema (Catalog #P3932, Sigma-Aldrich, St. Louis, Missouri) in 10 ml of 95% ethanol at 65°C for 8 h. Cell culture plates were coated with 1 ×PolyHema solution (12 mg/ml of 95% ethanol) overnight and washed with PBS the following day, before culturing cells (24). Cells were plated for 1, 3, and 24 h on PolyHema-coated dishes. Cell suspension was prepared as follows: cells were washed twice with PBS before dissociating them using 0.05% trypsin-ethylenediaminetetraacetic acid solution. Trypsin was neutralized by soybean trypsin inhibitor (Catalog #T9003, Sigma-Aldrich); cells were washed twice before plating on polyHema-coated dishes. Single-cell suspensions were obtained by adding 1 mmol/l ethylene glycol tetraacetic acid to DMEM medium.

METABOLIC STUDIES

All investigations of cellular metabolism were performed using DMEM medium (Catalog #17-207-CV, Corning) which does not contain glucose, pyruvate, or glutamine. At 24 h prior to experiments, culture medium was changed to DMEM (Catalog #17-207-CV, Corning) containing glutamine (2 mmol/l) and FBS (10%); glucose (25 mmol/l), pyruvate (25 mmol/l), or 25 mmol/l glucose + 1 mmol/l dimethyloxallyl glycine (DMOG) were added for the duration of experiment.

Cell metabolism was monitored using a Seahorse Bioscience XF instrument (Agilent Technologies, Santa Clara, California) (3,12,25). We measured the rate of change of dissolved O_2 in each well (oxygen consumption rate [OCR], which reflects OxPhos) and change in pH (extracellular acidification rate [ECAR], which reports glycolysis). A 96-well instrument (XF96) was used for monolayer samples and a 24-well instrument (XF24 with

Islet capture plates) was used for hydrogel (3D) samples (both Agilent Technologies). All experiments were repeated at least 3 times and were conducted using 6 replicates in each run.

Respiratory rates were measured as basal rates and after injection of inhibitors of the mitochondrial electron transport chain (ETC) or glycolysis. We used oligo (4 μmol/l) to inhibit mitochondrial F_1F_o-ATP synthase, rotenone (2 μmol/l) to inhibit Complex 1 of ETC, antimycin A (2 μmol/l) to inhibit complex 3 of ETC, FCCP (500 nmol/l) to uncouple mitochondria for quantification of maximum respiratory capacity, and iodo (100 μmol/l) to inhibit glycolysis (glyceraldehyde-3-phosphate dehydrogenase). The compounds were prepared as stock solutions and dissolved in the assay media immediately before the experiment.

To analyze energetics in suspension culture, Seahorse assay plates (Agilent Technologies) were coated with polyHema (Sigma), and cells were plated for 1 h prior to starting the assay.

Uncoupled respiration fraction was evaluated by adding FCCP after basal respiration measurements, followed by rotenone and antimycin A. Coupled respiration was evaluated by adding oligo after measuring basal respiration.

Respiration fractions were calculated as follows:

1. *Glycolytic reserve:* Increase in ECAR following inhibition of OxPhos by oligo.
2. *Glycolytic fraction:* ECAR fraction sensitive to iodo, calculated at 30 min after addition of iodo.
3. *Coupled respiration*: OCR sensitive to inhibition by oligo; it represents OCR used for phosphorylation of ADP in mitochondria.
4. *Uncoupled respiration*: FCCP-sensitive OCR; it reflects total mitochondrial reserve of OCR or maximal oxygen consumption capacity of mitochondria. FCCP was added after measuring basal respiration for calculation of uncoupled respiration.
5. *Total mitochondrial respiration*: OCR fraction sensitive to inhibition by rotenone + antimycin A.

The relative contribution of OxPhos versus glycolysis to cellular energetics was evaluated by computing OCR/ECAR ratios. One advantage of using this ratio over individual OCR and ECAR measurements is that it is independent of cell number—this is especially important in cell suspensions, because cell number in the measurement volume (transient microchamber) of the Seahorse XF sensor cartridge could vary between measurements.

Normalization of respiratory rates—Cells were lysed immediately after the Seahorse assay. Respiratory rates were normalized to cell number using the Picogreen DNA assay (Invitrogen, Carlsbad, California) following the manufacturer's instructions.

ATP MEASUREMENTS

ATP was measured using the ATP Determination Kit (A22066, Molecular Probes, Eugene, Oregon) and Veritas Luminometer (Turner BioSystems, Sunnyvale, California). Standard reaction solution was prepared according to instructions from the manufacturer for 100-μl reaction volume. Promega passive lysis buffer (Cat. # E1941, Promega, Madison, Wisconsin) was used to lyse the cells in each well for 25 min. The standard curve of known ATP concentration was prepared for each reaction. The signal in each well was normalized to cell number using the Picogreen DNA assay. ATP contribution was calculated as follows:

1. *Oligo-sensitive ATP %*: ATP levels in cells obtained after 30 to 45 min treatment with oligo. This fraction represents ATP produced by cells when OxPhos is inhibited. It does not represent total ATP produced by mitochondria, because a compensatory increase in glycolytic flux following inhibition of mitochondrial ATP synthase can increase cellular ATP generation by glycolysis. *OxPhos ATP percentage was calculated as follows:*

$$\text{Oligo}-\text{sensitive ATP}/\text{basal ATP} \times 100$$

2. *Iodo-sensitive ATP %*: We used this to calculate contribution of glycolysis to ATP production. This fraction represents ATP produced by cells when glycolysis is inhibited by iodo. Glycolytic ATP percentage is calculated as follows:

$$\text{Iodo}-\text{sensitive ATP}/\text{basal ATP} \times 100$$

3. *Oligo- and iodo-sensitive ^{99m}Tc-pertechnetate uptake* was used to calculate ^{99m}Tc-pertechnetate uptake after acute inhibition of OxPhos and glycolysis, respectively. NIS^{+}CDCs were treated with oligo or iodo and incubated with ^{99m}Tc-pertechnetate (11.1 kBq/ml) for 1 h, prior to washout of drug/radiotracer. Cells were subsequently lysed, and counts were recorded in a gamma-counter (PerkinElmer, Waltham, Massachusetts). Radioactivity in the samples was allowed to decay by storing them in the freezer at −20°C for 2 days prior to performing the Picogreen DNA assay. All experiments were repeated at least 3 times and conducted using 6 replicates in each run.

LACTATE MEASUREMENT

Because CO_2 generation by OxPhos can contribute to ECAR (16), we also measured lactate levels directly using the Lactate Assay Kit (ab65331, Abcam, Cambridge, United Kingdom). All experiments were repeated at least 3 times and conducted using 6 replicates in each run.

GLUCOSE UPTAKE

Fludeoxyglucose F18 (^{18}FDG) (74 kBq/ml) was added to cells for 1 h to measure glucose uptake. Counts were recorded in a gamma-counter (Perkin Elmer). Double-stranded DNA content was determined using the Quant-iT PicoGreen dsDNA Reagent and Kit (Invitrogen) to normalize results for cell number. All experiments were repeated at least 3 times and conducted using 6 replicates in each run.

PI3K-AKT INHIBITION

To evaluate the effect of Akt inhibition on cell metabolism and ^{99m}Tc-pertechnectate uptake, 10 μmol/l LY294002 (L9908, Sigma), a reversible PI3K inhibitor; 1 μmol/l Wortmannin (W1628, Sigma), an irreversible PI3K inhibitor; and 10 μmol/l MK-2206 (Selleck Chemical, Houston, Texas), a reversible Akt inhibitor were used.

HYDROGEL SYNTHESIS

HA:Bl:Ser hydrogels were prepared by mixing in 1:1 ratio, 10 w/v% hyaluronic acid (HA)–N-hydroxysuccinimide (NHS) (26) with equal volume of lysed rat blood and serum (1:1 ratio) containing CDCs. NHS groups in HA (hyaluronic acid) react with free amine groups present in serum, lysed blood, and myocardium to form amide bonds, resulting in injectable, porous hydrogels that can encapsulate cells and adhere to beating myocardium while permitting diffusion of metabolites and substrates (24). HA-NHS was dissolved in a medium containing glucose; thus, these hydrogels provide both adhesion motifs (27,28) and substrates (glucose, serum) to encapsulated cells. A detailed description of hydrogel synthesis is provided in the Supplemental Appendix.

SPECT IMAGING

To prove that in vivo ^{99m}Tc-pertechnetate uptake by transplanted NIS$^+$CDCs reflects cellular ATP levels, we performed in vivo SPECT imaging following 2 interventions that lead to opposite effects on CDC energetics, namely, hydrogel encapsulation (which boosts cellular ATP levels) and reversible Akt inhibition (which transiently reduces cellular ATP). To accomplish this goal, NIS$^+$CDCs (1×10^6) derived from syngeneic WK rats were transplanted epicardially into noninfarcted WK rats immediately after encapsulation in hydrogels. Dual isotope SPECT/CT imaging was performed at 1 and 24 h following transplantation. As described previously (3,20,25), ^{99m}Tc-pertechnetate and ^{201}TlCl were injected intravenously 1 h prior to imaging to visualize transplanted NIS$^+$CDCs and myocardium, respectively, by SPECT. Two groups of rats were studied: group 1 consisted of NIS$^+$CDCs encapsulated in hydrogels, and group 2 consisted of adherent NIS$^+$CDCs pre-treated with a reversible Akt inhibitor for 1 h followed by washout, prior to dissociation and encapsulation in hydrogels.

Please see the Supplemental Appendix for detailed methods for ^{18}FDG uptake, 2-photon microscopy, cell proliferation, cell surface glucose transporter 1 (GLUT1) expression, alpha$_5$ integrin localization, PI3K-AKT inhibition, hydrogel synthesis, animal surgery, SPECT image acquisition, and analyses.

STATISTICAL METHODS

Data was analyzed using GraphPad Prism (GraphPad Software, La Jolla, California). The Student *t* test or analysis of variance was used to analyze results of in vitro experiments, where data was normally distributed. The Mann-Whitney *U* test was performed to compare the in vivo SPECT signal at 1 h to the 24-h signal in the hydrogel + CDC and the hydrogel + CDC + Akt inhibitor groups. A value of $p < 0.05$ was used to reject the null hypothesis.

RESULTS

ADHERENT CELLS POSSESS GLYCOLYTIC RESERVE

We and others have demonstrated the importance of aerobic glycolysis in proliferating stem cells in culture (3,4,12,16). But, following transplantation into the heart, cells are exposed to blood whose composition is different from cell culture media. Furthermore, transplanted cells may also have limited access to O_2, as in the case of transplantation into ischemic tissue. Hence, we examined energy metabolism and quantified the relative contributions of OxPhos and glycolysis to cellular ATP generation under 3 metabolic states, namely aerobic glycolysis, anaerobic glycolysis, and OxPhos. We accomplished this by culturing adherent CDCs for 24 h in medium containing 10% FBS plus glucose (25 mmol/l) to favor aerobic glycolysis, pyruvate (25 mmol/l) to favor OxPhos, or glucose (25 mmol/l) + DMOG (1 mmol/l) (29) to favor anaerobic glycolysis, prior to metabolic studies (Figure 1A).

During aerobic glycolysis, OxPhos inhibition by oligo resulted in a 55% reduction in OCR (coupled respiration = 55%) (Figures 1B and 1C), which was associated with a small drop in cellular ATP levels (OxPhos ATP = 15%) (Figure 1D). This reduction in OCR was associated with a rapid increase (within minutes) in ECAR (Figure 1B) as well as an increase in glucose uptake and lactate generation (Figure 1E), indicating the presence of *glycolytic reserve* (13–15). Iodo treatment led to a marked reduction in ECAR and cellular ATP levels (glycolytic ATP = 85%), confirming a reliance on glycolysis for ATP generation in adherent cells (Figure 1D). As expected, oligo led to abolition of OCR and collapse of cellular ATP in the pyruvate condition (OxPhos ATP = 100%), but had no effect on OCR and cellular ATP during anaerobic glycolysis; however, iodo led to a marked reduction in cellular ATP during anaerobic glycolysis (glycolytic ATP = 100%) and had no effect in the pyruvate condition (glycolytic ATP = 0%) (Figures 1C and 1D). Taken together, these results indicate that OxPhos contributes ~15% of cellular ATP and glycolysis contributes ~85% of ATP in adherent CDCs under routine culture conditions (Figure 1D).

Next, we examined whether inhibiting OxPhos or glycolysis affected mitochondrial membrane potential ($\Delta\Psi_m$), which is an indicator of mitochondrial energetics and cell viability. Mitochondrial membrane potential was maintained after oligo treatment (for 24 h) during aerobic and anaerobic glycolysis, but not in pyruvate medium, indicating that glycolytic ATP can maintain cell viability in adherent cells during aerobic glycolysis (Figure 1F). Interestingly, cell proliferation was observed for 6 days following OxPhos inhibition by oligo in the setting of aerobic glycolysis (Figure 1G), but not in the pyruvate condition (despite maintenance of cellular ATP levels in the pyruvate condition), confirming the importance of glycolysis in the maintenance of cell proliferation.

DETERMINANTS OF GLYCOLYTIC RESERVE

Because a compensatory increase in ECAR occurred within minutes of inhibiting OxPhos, we investigated post-translational changes in signaling pathways involved in energy sensing (AMP Kinase [30]) and regulation of metabolism (Akt [31,32], HIF-1α [33]) as possible mediators of glycolytic up-regulation. We found no evidence for HIF-1α stabilization by western blot following oligo treatment (Supplemental Figure 1). A time course analysis of

Akt and AMPK phosphorylation over 24 h, following oligo treatment in the 3 metabolic states (Figure 1H) revealed that p-AMPK peaked at 30 min and declined to baseline levels at 60 min during aerobic glycolysis; reduction in p-AMPK was associated with an increase in p-Akt. In contrast, oligo had no effect on AMPK and Akt signaling during anaerobic glycolysis (DMOG), but resulted in sustained increase in AMPK phosphorylation (activation), Akt dephosphorylation (inhibition), depolarization of $\Delta\Psi_m$ (Figure 1F), and cell death (at 6 h) in pyruvate medium (Figure 1G). Taken together, our results suggest a role for Akt signaling in glycolytic reserve.

Next, we tested the hypothesis that Akt inhibition would abolish glycolytic reserve. Reversible inhibition of PI3K and Akt was accomplished using Ly294002 (10 μmol/l) and MK2206 (10 μmol/l), respectively, and irreversible PI3K inhibition was achieved by Wortmannin (1 mmol/l) (Supplemental Figure 2A). The most significant effect of PI3K-Akt inhibition was on glycolysis: we observed a marked reduction in ECAR (Figure 2A), glucose uptake (Figure 2C), lactate generation (Figure 2D), and loss of glycolytic reserve (manifested by lack of compensatory increase in ECAR [Figures 2A and 2B] and collapse of $\Delta\Psi_m$ after OxPhos inhibition by oligo [Supplemental Figure 2B]). PI3K-Akt inhibition also led to a small reduction in OCR (Figure 2A) and decrease in total cellular ATP levels (Figure 2B).

To examine mechanisms underlying reduction in glucose uptake, we used flow cytometry to quantify cell surface expression of GLUT1, the main glucose transporter in CDCs (Supplemental Figure 3A), whose translocation to the membrane has been reported to be dependent on Akt signaling (34). Using a GLUT1 construct containing a FLAG tag (Supplemental Figure 3B), we observed that oligo treatment increased cell surface localization of FLAG-GLUT1 (Figure 2E), and PI3K-Akt inhibition reduced cell surface expression of GLUT1 (34). These results confirm the importance of Akt signaling in preserving glucose uptake, glycolysis, and glycolytic reserve in adherent cells.

Last, we investigated the role of serum (35) on glycolytic reserve in adherent CDCs. We studied serum because it is an important component of cell culture medium that can activate Akt signaling. Serum withdrawal for 24 h led to an increase in OCR/ECAR ratio (Figure 3A), but total cellular ATP levels were lower (Figure 3B) when compared with the serum-containing condition. Serum withdrawal led to energetic stress, manifested by AMPK activation and Akt dephosphorylation (Figure 3C). These results indicate the importance of serum in maintenance of energy metabolism in adherent CDCs.

LARGE GLYCOLYTIC RESERVE IS PRESENT IN ADULT STEM CELLS

To assess the presence of glycolytic reserve in other cell types, we performed limited metabolic studies in human adipocyte stromal cells (ASCs) (11), human bone marrow–derived MSCs and NRVMs (Figures 4A and 4D, Supplemental Figures 4A and 4B). OxPhos inhibition led to a compensatory increase in ECAR and glycolytic ATP generation, but had no effect on ΔΨm, indicating the presence of glycolytic reserve in ASCs. Coupled respiration was similar in MSCs, ASCs, and CDCs, but was significantly higher in NRVMs. Furthermore, glycolysis (ECAR) was higher in MSCs, ASCs, and CDCs, when compared with NRVMs (Figure 4D). Next, we used MitoTracker Green (Thermo Fisher), which labels

mitochondria independent of ΔΨm to estimate mitochondrial number (36) in CDCs, ASCs, MSCs, and NRVMs (Supplemental Figure 4C), by flow cytometry. NRVMs had the highest numbers of mitochondria followed by CDCs, ASCs, and MSCs. These results would explain higher mitochondrial respiration in NRVMs when compared with CDCs, ASCs, and MSCs.

Taken together, our studies in adherent adult stem cells indicate the presence of a large glycolytic reserve. This glycolytic reserve capacity can maintain cellular ATP/viability/proliferation following OxPhos inhibition, requires Akt activation, and is independent of HIF-1α stabilization.

CELL DISSOCIATION AND SUSPENSION LEAD TO LOSS OF GLYCOLYTIC RESERVE AND RELIANCE ON OxPhos FOR ATP GENERATION

Because cell dissociation and suspension are prerequisites for most studies of stem cell transplantation, we investigated the effect of cell suspension on energy metabolism. We have previously reported that cell suspension down-regulates cellular glucose uptake and ATP levels, but the mechanisms underlying these results have not been elucidated. In this study, CDCs were dissociated and plated on polyHema-coated plates (that prevent cell adhesion) for the suspension condition, or on TC-treated plates that promote cell adhesion for the adherent condition. Energetic parameters were monitored over the course of 3 h (Figure 5A). Cell dissociation/suspension reduced glycolysis and abolished glycolytic reserve (Figure 5A1). The OCR/ECAR ratio (Figure 5B) was increased in suspension due to a small increase in OxPhos and marked reduction in glycolysis (Figures 5A1 and 5A2). Notably, total cellular ATP was reduced despite enhanced ATP generation by OxPhos (oligo-sensitive ATP) (Figure 5C1), indicating that the small increase in OCR is unable to compensate for reduced ATP generation by glycolysis. Presence of serum in the cell suspension medium enhanced ATP generation by OxPhos, resulting in higher total ATP levels compared with serum-free conditions (Figure 5C1). In contrast, OxPhos inhibition by oligo led to marked reduction in cellular ATP (Figure 5C1) despite the presence of serum/glucose, indicating the importance of OxPhos for ATP generation in suspension. To investigate mechanisms underlying reduction of glycolysis during cell suspension, we measured glucose uptake and cell surface GLUT1 in suspended cells. Glucose uptake (Figure 5D) and cell surface GLUT1 levels (Figure 5D) were reduced with cell suspension. We observed progressive reduction in cell surface GLUT1 (Figure 5E) and ΔΨm loss (Supplemental Figure 5) with longer periods (3 to 6 h) of cell suspension, indicating that nutrient limitation in the presence of glucose as substrate could underlie energetic stress in suspension.

Because ATP generation by OxPhos is increased in suspension, we tested the hypothesis that up-modulation of OxPhos would reduce energetic stress and improve viability in suspension. We replaced glucose with pyruvate because it is transported into cells via the monocarboxylate transporter (37) rather than GLUT1, and can directly enter the Krebs cycle to stimulate OxPhos, thus bypassing glycolysis. We discovered that both cellular ATP levels (Figure 5C1) and viability (Figures 5F and 5G) were markedly higher in pyruvate-treated suspended cells when compared with cells suspended in glucose media. Similarly, serum containing fatty acids and growth factors (35) also stimulated OxPhos and increased cellular ATP levels and viability of suspended cells (Figures 5F and 5G). In contrast, OxPhos

inhibition by oligo or antimycin A markedly reduced cellular ATP levels and cell viability in suspension, indicating the importance of OxPhos in suspended cells (Figures 5F and 5G). Akt inhibition (MK2206) also reduced viability, indicating the importance of Akt signaling in maintenance of viability in suspension (Figure 5F). Viability was similar at 1 h in the presence or absence of glucose (Figure 5F), which could be attributed to very low glucose uptake by suspended cells.

Our results using suspended cells indicate that cell dissociation/suspension results in nutrient limitation in the presence of glucose, a switch toward OxPhos for energetic needs, and reduction in cellular ATP/viability, which can be partially rescued by up-modulating OxPhos using pyruvate or serum.

RAPID ACTIVATION OF CELL ADHESION RELIEVES ENERGETIC STRESS, RESTORES GLYCOLYTIC RESERVE AND IMPROVES VIABILITY OF SUSPENDED CDCs

Because bypassing glycolysis with pyruvate/serum improved viability but did not restore energy metabolism in suspended cells, we hypothesized that activation of cell adhesion is essential for restoration of energetics in CDCs. To test this hypothesis, we investigated energetics after plating cells as monolayers (2D) or encapsulation in 3D scaffolds (that could be used to deliver cells in vivo). We designed scaffolds (HA:Bl:Ser hydrogels) containing serum/lysed blood, which provide adhesion motifs (RGD/arginyl-glycylaspartic acid [38]) to encapsulated cells. Rapid activation of cell adhesion following plating as monolayers and encapsulation in hydrogels was confirmed using CHO cells expressing α_5 integrin-eGFP (39): integrin was primarily localized to the cell membrane within 1 to 3 h in 2D monolayers and encapsulated cells, but not in suspended cells (Figure 6A). Western blot confirmed activation of Akt signaling within 1 h of replating as 2D monolayers or following encapsulation in hydrogels (Supplemental Figure 6).

Replating cells as monolayers (2D) in serum/glucose-containing medium led to restoration of cellular ATP levels within 3 h (Figure 5C3). OCR/ECAR ratio and ATP generation by OxPhos (OxPhos ATP%) at 1 h after replating were higher than cells adherent for 24 h (Figure 5C2), indicating increased utilization of OxPhos for ATP generation early in the adhesion process. Glycolytic ATP generation and glycolytic reserve (Figure 5C) were restored within 3 h of replating.

CDC encapsulation in (3D) hydrogels stimulated OxPhos and glycolysis (Figure 6B); increased OCR/ECAR ratio (Figure 6C), glucose uptake (Figure 6D), and cellular ATP levels; and restored glycolytic reserve (namely, glycolytic ATP generation [Figure 6E] and maintenance of $\Delta\Psi_m$ following inhibition of OxPhos by oligo [Figure 6F]) within 1 to 3 h of encapsulation. Notably, encapsulation in HA:Bl:Ser hydrogels led to Akt activation (Supplemental Figure 5) and higher glucose uptake and cellular ATP levels than plating as monolayers (Figures 6D and 6E), suggesting that the 3D environment provided by our scaffolds is ideal for rapid restoration of stem cell energetics.

Taken together, our results indicate that the contribution of OxPhos to ATP generation is high early during the adhesion process, which could underlie the rapid relief of energetic deficits incurred during cell suspension.

IN VIVO ^{99m}Tc-PERTECHNETATE UPTAKE BY NIS^{+}CDCs REPORTS TRANSPLANTED CELL ENERGETICS

In vivo molecular imaging studies are needed to translate basic metabolic studies into the clinical arena. Several groups have demonstrated the utility of NIS as a reporter of cell engraftment (3,20,40), but detailed studies of NIS as a metabolic reporter gene are lacking. Because ^{99m}Tc-pertechnetate uptake by NIS is coupled to Na^+ uptake, which depends on the intracellular Na^+ gradient and Na^+-K^+-ATPase activity (41) (Figure 7A), we expected that cellular ^{99m}Tc-pertechnetate uptake would vary with cellular ATP levels. To confirm dependence of ^{99m}Tc-pertechnetate uptake on cellular ATP levels, we quantified ^{99m}Tc-pertechnetate in NIS^{+}CDCs after restricting metabolism to aerobic glycolysis (glucose medium), OxPhos (pyruvate medium), or anaerobic glycolysis (DMOG + glucose), and following treatment with metabolic inhibitors. We calculated oligo-sensitive ^{99m}Tc-pertechnetate uptake and compared it with oligo-sensitive cellular ATP levels. Notably, the fraction of ^{99m}Tc-pertechnetate uptake inhibited by oligo (oligo-sensitive ^{99m}Tc-pertechnetate uptake) (Figures 7B and 7C) was similar to the fraction of cellular ATP inhibited by oligo (oligo-sensitive ATP levels) (Figure 1D), indicating that ^{99m}Tc-pertechnetate uptake by NIS^{+} cells mirrors cellular ATP levels.

Next, we assessed in vitro ^{99m}Tc-pertechnetate uptake following NIS^{+}CDC encapsulation in hydrogels. CDCs grown as monolayers were compared with CDCs encapsulated in hydrogels and suspended CDCs. ^{99m}Tc-pertechnetate (Figure 7D) uptake by CDCs encapsulated in hydrogels was significantly higher than suspended CDCs or CDCs plated as monolayers.

We have previously shown that intramyocardial transplantation of suspended cells (which have low cellular ATP levels) leads to very low ^{99m}Tc-pertechnetate uptake (SPECT signal) at 1 to 3 h post-transplantation, with higher SPECT signal at 24 h post-transplantation (6). To prove that in vivo ^{99m}Tc-pertechnetate uptake by SPECT imaging is modulated by cellular ATP levels, we performed SPECT imaging of transplanted NIS^{+}CDCs encapsulated in HA:Bl:Ser hydrogels at 1 to 3 h and 24 h post-transplantation. SPECT imaging of NIS^{+}CDCs encapsulated in hydro-gels resulted in high ^{99m}Tc-pertechnetate uptake at 1 to 3 h following transplantation, which was similar to ^{99m}Tc-pertechnetate uptake at 24h (Figures 8B1 and 8C), reflecting rapid hydrogel-mediated restoration of energetics post-transplantation. In contrast, transient Akt inhibition prior to encapsulation/transplantation resulted in lower SPECT signal at 1 to 3 h (Figure 8B2) when compared with 24 h, a trend that resembled transplantation of suspended cells (3) (Figure 8D). In vitro studies confirmed transient suppression of energetics and ATP generation (Supplemental Figures 7A and 7B) as well as lower in vitro ^{99m}Tc-pertechnetate uptake (Supplemental Figure 7C) in NIS^{+}CDCs pre-treated with a reversible Akt inhibitor when compared with untreated cells.

DISCUSSION

CDCs HAVE METABOLIC FLEXIBILITY

A novel result of our study is that CDCs have metabolic flexibility that is influenced by cell adhesion status (Figure 9). Adherent CDCs utilize both glycolysis and OxPhos to generate

ATP, but the contribution of glycolysis exceeds that of OxPhos. Use of both OxPhos and glycolysis for ATP generation would be advantageous for in vivo engrafted CDCs because, unlike the cell culture environment where cells are constantly bathed in 25 mmol/l glucose, exclusive dependence on glycolysis in vivo where physiological glucose concentrations are lower (3.9 to 7.2 mmol/l), could lead to substrate limitation. In contrast to the adherent condition, cell dissociation and suspension increase reliance on OxPhos for ATP generation and viability and lead to energetic stress, despite the fact that OxPhos is more efficient in generating ATP than glycolysis (OxPhos: 30 to 36 ATP/glucose vs. glycolysis: 2 ATP/glucose). The metabolic bottleneck in suspended CDCs appears to be at the level of glucose uptake, because stimulation of OxPhos using pyruvate or serum increases cellular ATP levels and viability in suspension. It is important to note that ATP levels are only restored upon activation of cell adhesion. Hence, rapid activation of in vivo cell adhesion would be expected to increase transplanted cell engraftment and cardiac repair. We accomplished this by encapsulating CDCs in HA:Bl:Ser hydrogels that provide adhesion motifs (RGD) and substrates (serum/glucose) and thus, restore cellular energetics and glycolytic reserve within 3 h of cell transplantation. Notably, OxPhos and glycolysis were markedly higher when CDCs were cultured in hydrogels (3D culture), when compared with CDCs plated as monolayers (2D culture)—this result could be mediated by greater numbers of adhesion sites presented in 3D hydrogels, combined with stimulatory effects bestowed by serum and glucose availability. Furthermore, 3D cell culture could be more physiological than 2D cell culture as monolayers, because the in vivo environment is 3D (42).

GLYCOLYTIC RESERVE

The ideal metabolic profile to promote survival of transplanted CDCs would be reliance on glycolysis for energetic needs, because local injury or edema following injection could result in limited O_2 delivery to transplanted cells acutely. Glycolytic reserve, namely, the capacity to increase glycolytic flux following inhibition of OxPhos, is a characteristic of adherent proliferating cells (13–15) that would permit transplanted cell survival and proliferation following transplantation. Our study revealed that glycolytic reserve is maintained by post-translational mechanisms, namely Akt phosphorylation. However, Akt phosphorylation alone may be unable to explain the rapid increase in ECAR within 5 min of oligo treatment. A possible mechanism underlying the rapid increase in ECAR is competition between pyruvate kinase and mitochondria for ADP phosphorylation (6): net glycolytic ATP generation occurs in the thermodynamically highly favorable reaction catalyzed by pyruvate kinase ($\Delta G0 = -61$ kJ/mol) (43). Inhibition of mitochondrial ATP generation would increase ADP availability, thus increasing pyruvate kinase activity, leading to a rapid increase in glycolytic flux. Based on results from previous studies (13–15), ATP generation by increased glycolytic flux, combined with glycolytic intermediates (e.g., glucose-6-p) and metabolites from the pentose-phosphate pathway probably underlie maintenance of cell viability and proliferation following OxPhos inhibition.

In anaerobic glycolysis, OxPhos is inhibited by HIF-1α (33) at the pyruvate dehydrogenase step. HIF-1α stabilization by hypoxia or DMOG led to up-regulation of Akt phosphorylation, glucose uptake, ECAR, and lactate generation, while maintaining cellular ATP. Similar increases in glucose uptake, ECAR, and lactate generation were observed

following oligo treatment during aerobic glycolysis. These results indicate that up-regulation of glycolysis in adherent CDCs can occur via HIF-1α–dependent and –independent mechanisms.

IN VIVO SPECT IMAGING

This study demonstrates that SPECT, which is a widely available clinical imaging modality, and ^{99m}Tc-pertechnetate, a clinically approved tracer, could be used in conjunction with NIS gene expression to monitor/maximize energetics and thus increase engraftment of transplanted cells in future preclinical studies of cell transplantation. We have previously demonstrated, using SPECT imaging, that intramyocardial transplantation of suspended cells leads to a low SPECT signal at 1 to 3 h post-transplantation (when compared with 24 h) (3), whereas cell encapsulation in HA:Ser hydrogels prior to epicardial transplantation leads to a high SPECT signal (similar to 24 h signal) (25). We attributed differences in the SPECT signal early post-transplantation in the suspended and hydrogel conditions to differences in cellular energetics, but direct proof for this hypothesis was lacking. In the current study, we used a combination of in vitro studies of ^{99m}Tc-pertechnetate uptake and in vivo studies, where ATP levels were modulated in NIS^{+}CDCs encapsulated in hydrogels prior to epicardial transplantation, to illustrate dependence of ^{99m}Tc-pertechnetate uptake (SPECT signal) on cellular ATP levels. In contrast to our previous study (25), which focused on the use of HA:Ser hydrogels to promote cardiac regeneration, our current study was geared toward a comprehensive investigation of metabolism, its regulation, and identification of metabolic strategies that could boost energetics and viability of transplanted cells.

STUDY LIMITATIONS

Most of the studies were performed in CDCs because of ease of transduction by lentivirus and optimization of in vivo imaging of CDCs in syngeneic WK rats (3). Importantly, our limited in vitro studies in other cell types, such as human MSCs and ASCs, suggest that our results could be extrapolated to cell types that are currently in use to promote regeneration in the heart and other organs. Here, we provide proof-of-principle results for the use of scaffolds to restore transplanted cell energetics acutely following transplantation. One limitation of using hydrogels containing serum or lysed blood is interindividual variations in serum/blood composition that can influence stem cell biology; metabolic scaffolds with a defined chemical composition would be optimal for clinical translation. Last, we recognize that the effect of metabolic modulation on exosome release was not assessed in this study. Because exosome secretion is an important mechanism underlying the benefits of CDC transplantation (44), our study has unclear implications for exosome release in particular, and for CDC potency in general.

CONCLUSIONS

The data presented herein unveil the metabolic flexibility exhibited by CDCs and ASCs, along with the important role of adhesion in the regulation of cellular energetics. Adherent cells possess glycolytic reserve that is maintained by Akt signaling. In contrast, cells in suspension experience nutrient limitation due to down-regulation of glucose uptake, and rely on OxPhos for ATP generation and viability. Rapid activation of cell adhesion using

scaffolds restores energetics and thus holds great promise for improving transplanted cell engraftment.

Supplementary Material

Refer to Web version on PubMed Central for supplementary material.

Acknowledgments

This work was funded by the American Heart Association (AHA-BGIA and AHA-GIA) and the National Institutes of Health (NIH (RO1 HL092985 and UL1 RR 025005). Dr. Chan was supported by NIH. Training Grant NIHT32HL07227. Dr. Karakas was supported by a TUBITAK2219 Research Programme Grant and Fulbright Grant. Dr. Woldemichael was supported by NIH Diversity Fellowships (R01HL092985). Dr. Vakrou was supported by a fellowship from the Hellenic Heart Failure Society. Dr. Tsui has received a royalty from GE Healthcare; and has received a research contract from Philips Healthcare. All other authors have reported that they have no relationships relevant to the contents of this paper to disclose. Drs. Afzal and Chan contributed equally to this work. Robert Roberts, MD, served as Guest Editor for this paper.

APPENDIX

For an expanded Methods section and supplemental figures, please see the online version of this article.

ABBREVIATIONS AND ACRONYMS

ANOVA	analysis of variance
CDC	cardiosphere-derived cells
DMOG	dimethyloxallyl glycine
ECAR	extracellular acidification rate
GLUT1	glucose transporter 1
iodo	iodoacetate
OCR	oxygen consumption rate
oligo	oligomycin
OxPhos	oxidative phosphorylation

References

1. Laflamme MA, Chen KY, Naumova AV, et al. Cardiomyocytes derived from human embryonic stem cells in pro-survival factors enhance function of infarcted rat hearts. Nat Biotechnol. 2007; 25:1015–24. [PubMed: 17721512]
2. Schafer ZT, Grassian AR, Song L, et al. Antioxidant and oncogene rescue of metabolic defects caused by loss of matrix attachment. Nature. 2009; 461:109–13. [PubMed: 19693011]
3. Chang C, Chan A, Lin X, et al. Cellular bioenergetics is an important determinant of the molecular imaging signal derived from luciferase and the sodium-iodide symporter. Circ Res. 2013; 112:441–50. [PubMed: 23255420]
4. Fillmore N, Huqi A, Jaswal JS, et al. Effect of fatty acids on human bone marrow mesenchymal stem cell energy metabolism and survival. PLoS One. 2015; 10:e0120257. [PubMed: 25768019]

5. Vander Heiden MG, Cantley LC, Thompson CB. Understanding the Warburg effect: the metabolic requirements of cell proliferation. Science. 2009; 324:1029–33. [PubMed: 19460998]
6. Melo RF, Stevan FR, Campello AP, Carnieri EG, de Oliveira MB. Occurrence of the Crabtree effect in HeLa cells. Cell Biochem Funct. 1998; 16:99–105. [PubMed: 9636997]
7. Makkar RR, Smith RR, Cheng K, et al. Intra-coronary cardiosphere-derived cells for heart regeneration after myocardial infarction (CADUCEUS): a prospective, randomised phase 1 trial. Lancet. 2012; 379:895–904. [PubMed: 22336189]
8. Smith RR, Barile L, Cho HC, et al. Regenerative potential of cardiosphere-derived cells expanded from percutaneous endomyocardial biopsy specimens. Circulation. 2007; 115:896–908. [PubMed: 17283259]
9. Cheng K, Malliaras K, Smith RR, et al. Human cardiosphere-derived cells from advanced heart failure patients exhibit augmented functional potency in myocardial repair. J Am Coll Cardiol HF. 2014; 2:49–61.
10. Chimenti I, Smith RR, Li TS, et al. Relative roles of direct regeneration versus paracrine effects of human cardiosphere-derived cells transplanted into infarcted mice. Circ Res. 2010; 106:971–80. [PubMed: 20110532]
11. Gimble JM, Katz AJ, Bunnell BA. Adipose-derived stem cells for regenerative medicine. Circ Res. 2007; 100:1249–60. [PubMed: 17495232]
12. Reid B, Afzal JM, McCartney AM, Abraham MR, O'Rourke B, Elisseeff JH. Enhanced tissue production through redox control in stem cell-laden hydrogels. Tissue Eng Part A. 2013; 19:2014–23. [PubMed: 23627869]
13. Hao W, Chang CP, Tsao CC, Xu J. Oligomycin-induced bioenergetic adaptation in cancer cells with heterogeneous bioenergetic organization. J Biol Chem. 2010; 285:12647–54. [PubMed: 20110356]
14. Lanning NJ, Looyenga BD, Kauffman AL, et al. A mitochondrial RNAi screen defines cellular bioenergetic determinants and identifies an adenylate kinase as a key regulator of ATP levels. Cell Rep. 2014; 7:907–17. [PubMed: 24767988]
15. Hill BG, Benavides GA, Lancaster JR Jr, et al. Integration of cellular bioenergetics with mitochondrial quality control and autophagy. Biol Chem. 2012; 393:1485–512. [PubMed: 23092819]
16. Mookerjee SA, Nicholls DG, Brand MD. Determining maximum glycolytic capacity using extracellular flux measurements. PLoS One. 2016; 11:e0152016. [PubMed: 27031845]
17. Zhang Z, Vuori K, Reed JC, Ruoslahti E. The alpha 5 beta 1 integrin supports survival of cells on fibronectin and up-regulates Bcl-2 expression. Proc Natl Acad Sci U S A. 1995; 92:6161–5. [PubMed: 7541142]
18. Giancotti FG, Ruoslahti E. Integrin signaling. Science. 1999; 285:1028–32. [PubMed: 10446041]
19. Hynes RO. Integrins: bidirectional, allosteric signaling machines. Cell. 2002; 110:673–87. [PubMed: 12297042]
20. Terrovitis J, Kwok KF, Lautamaki R, et al. Ectopic expression of the sodium-iodide symporter enables imaging of transplanted cardiac stem cells in vivo by single-photon emission computed tomography or positron emission tomography. J Am Coll Cardiol. 2008; 52:1652–60. [PubMed: 18992656]
21. Dai G, Levy O, Carrasco N. Cloning and characterization of the thyroid iodide transporter. Nature. 1996; 379:458–60. [PubMed: 8559252]
22. Messina E, De Angelis L, Frati G, et al. Isolation and expansion of adult cardiac stem cells from human and murine heart. Circ Res. 2004; 95:911–21. [PubMed: 15472116]
23. Abraham MR, Henrikson CA, Tung L, et al. Antiarrhythmic engineering of skeletal myoblasts for cardiac transplantation. Circ Res. 2005; 97:159–67. [PubMed: 15976318]
24. Kantak SS, Kramer RH. E-cadherin regulates anchorage-independent growth and survival in oral squamous cell carcinoma cells. J Biol Chem. 1998; 273:16953–61. [PubMed: 9642258]
25. Chan AT, Karakas MF, Vakrou S, et al. Hyaluronic acid-serum hydrogels rapidly restore metabolism of encapsulated stem cells and promote engraftment. Biomaterials. 2015; 73:1–11. [PubMed: 26378976]

26. Chang CY, Chan AT, Armstrong PA, et al. Hyaluronic acid-human blood hydrogels for stem cell transplantation. Biomaterials. 2012; 33:8026–33. [PubMed: 22898181]
27. Fujita Y, Kitagawa M, Nakamura S, et al. CD44 signaling through focal adhesion kinase and its anti-apoptotic effect. FEBS Lett. 2002; 528:101–8. [PubMed: 12297287]
28. Gerecht S, Burdick JA, Ferreira LS, Townsend SA, Langer R, Vunjak-Novakovic G. Hyaluronic acid hydrogel for controlled self-renewal and differentiation of human embryonic stem cells. Proc Natl Acad Sci U S A. 2007; 104:11298–303. [PubMed: 17581871]
29. Lu H, Dalgard CL, Mohyeldin A, McFate T, Tait AS, Verma A. Reversible inactivation of HIF-1 prolyl hydroxylases allows cell metabolism to control basal HIF-1. J Biol Chem. 2005; 280:41928–39. [PubMed: 16223732]
30. Hardie DG. AMP-activated protein kinase: an energy sensor that regulates all aspects of cell function. Genes Dev. 2011; 25:1895–908. [PubMed: 21937710]
31. Manning BD, Cantley LC. AKT/PKB signaling: navigating downstream. Cell. 2007; 129:1261–74. [PubMed: 17604717]
32. Elstrom RL, Bauer DE, Buzzai M, et al. Akt stimulates aerobic glycolysis in cancer cells. Cancer Res. 2004; 64:3892–9. [PubMed: 15172999]
33. Kim JW, Tchernyshyov I, Semenza GL, Dang CV. HIF-1-mediated expression of pyruvate dehydrogenase kinase: a metabolic switch required for cellular adaptation to hypoxia. Cell Metab. 2006; 3:177–85. [PubMed: 16517405]
34. Wieman HL, Wofford JA, Rathmell JC. Cytokine stimulation promotes glucose uptake via phosphatidylinositol-3 kinase/Akt regulation of Glut1 activity and trafficking. Mol Biol Cell. 2007; 18:1437–46. [PubMed: 17301289]
35. Brunner D, Frank J, Appl H, Schoffl H, Pfaller W, Gstraunthaler G. Serum-free cell culture: the serum-free media interactive online database. ALTEX. 2010; 27:53–62. [PubMed: 20390239]
36. Woldt E, Sebti Y, Solt LA, et al. Rev-erb-alpha modulates skeletal muscle oxidative capacity by regulating mitochondrial biogenesis and autophagy. Nat Med. 2013; 19:1039–46. [PubMed: 23852339]
37. Halestrap AP, Price NT. The proton-linked monocarboxylate transporter (MCT) family: structure, function and regulation. Biochem J. 1999; 343(Pt 2):281–99. [PubMed: 10510291]
38. D'Souza SE, Ginsberg MH, Plow EF. Arginylglycyl-aspartic acid (RGD): a cell adhesion motif. Trends Biochem Sci. 1991; 16:246–50. [PubMed: 1926332]
39. Laukaitis CM, Webb DJ, Donais K, Horwitz AF. Differential dynamics of alpha 5 integrin, paxillin, and alpha-actinin during formation and disassembly of adhesions in migrating cells. J Cell Biol. 2001; 153:1427–40. [PubMed: 11425873]
40. Ruben E, Jamai A, Afzal J, et al. Genomic analysis of the rhg1 locus: candidate genes that underlie soybean resistance to the cyst nematode. Mol Genet Genomics. 2006; 276:503–16. [PubMed: 17024428]
41. Penheiter AR, Russell SJ, Carlson SK. The sodium iodide symporter (NIS) as an imaging reporter for gene, viral, and cell-based therapies. Curr Gene Ther. 2012; 12:33–47. [PubMed: 22263922]
42. Baker BM, Chen CS. Deconstructing the third dimension: how 3D culture microenvironments alter cellular cues. J Cell Sci. 2012; 125:3015–24. [PubMed: 22797912]
43. Lehninger, AL., Nelson, DL., Cox, MM. Lehninger principles of biochemistry. 6th. New York, NY: W.H. Freeman; 2013.
44. Ibrahim AG, Cheng K, Marban E. Exosomes as critical agents of cardiac regeneration triggered by cell therapy. Stem Cell Reports. 2014; 2:606–19. [PubMed: 24936449]

HIGHLIGHTS

- Cell adhesion status regulates energy metabolism in adult stem cells
- Adherent adult stem cells (CDCs, MSCs, ASCs) utilize glycolysis to generate majority (70% to 85%) of their cellular ATP needs
- Akt phosphorylation transduces adhesion-mediated regulation of energy metabolism by regulating membrane translocation of glucose transporters (GLUT1) and thus, cellular glucose uptake and glycolysis
- Cell dissociation/suspension leads to Akt de-phosphorylation, >3-fold reduction in the number of cell surface GLUT1 receptors, downregulation of cellular glucose uptake, glycolysis, cellular ATP levels, and loss of cell viability
- Encapsulation of dissociated cells in hydrogels that provide cell adhesion motifs, promotes Akt phosphorylation, rapidly restores glycolysis, and cellular ATP levels
- ^{99m}Tc-pertechnetate uptake (by cells genetically engineered to express the Na-Iodide symporter) reflects cellular ATP levels, thus permitting in vivo monitoring of energetics of transplanted cells by SPECT imaging.

PERSPECTIVES

COMPETENCY IN MEDICAL KNOWLEDGE

Despite the remarkable regenerative potential of stem/progenitor cells, the functional benefits of cell therapy when assessed by changes in ejection fraction is small. Low levels of transplanted cell survival are an important contributory factor. Increase in engraftment levels would be expected to increase functional benefits of therapy.

TRANSLATIONAL OUTLOOK

The results from this study also suggests that metabolic modulation of suspended cells using substrates such as pyruvate (that bypass glycolysis) and metabolic scaffolds that promote cell adhesion and activate Akt signaling hold promise for improving transplanted cell engraftment. A combination of metabolic modulation with in vivo molecular imaging in preclinical large animal models is needed prior to clinical translation.

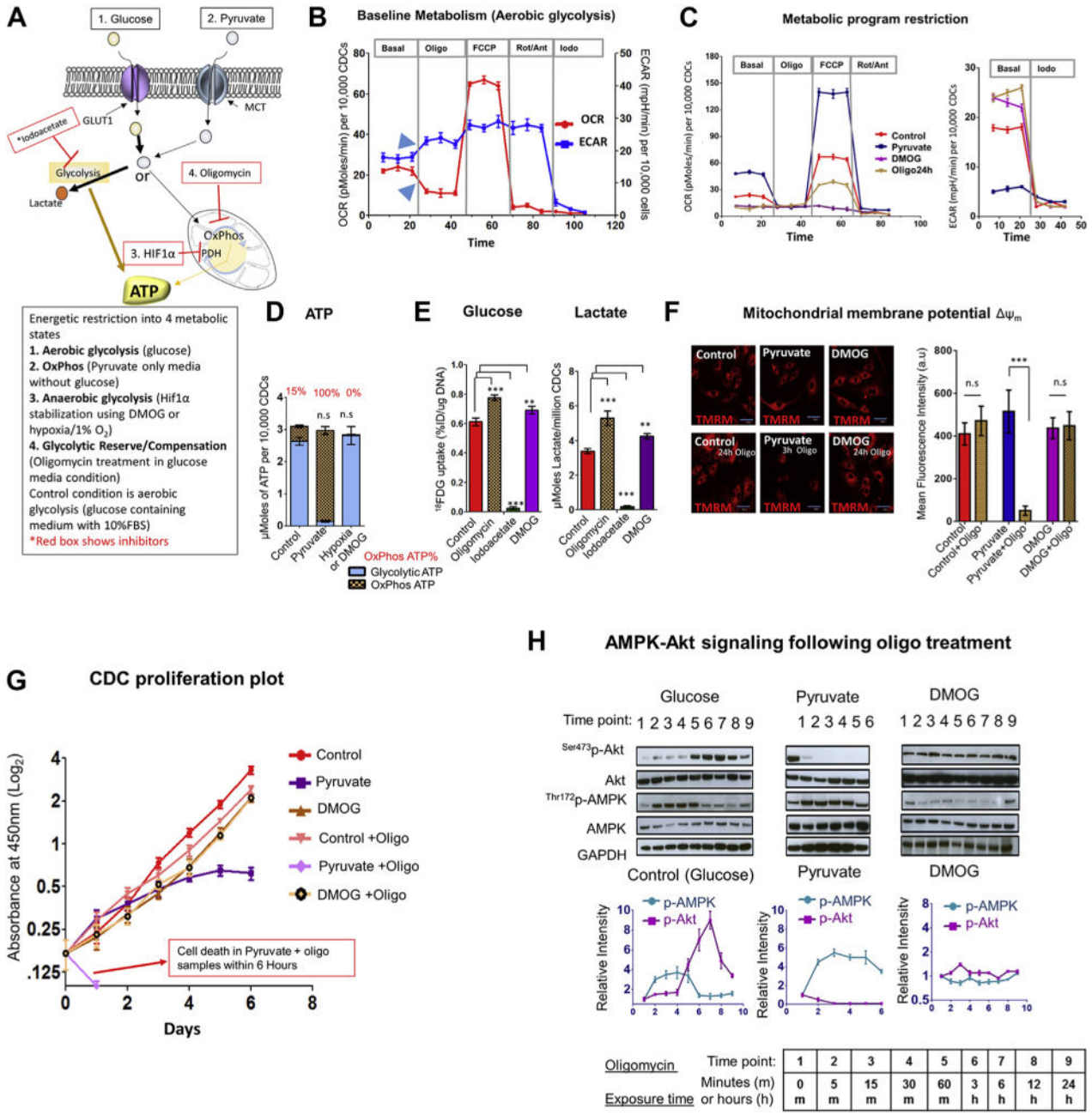

FIGURE 1. Metabolic Restriction in CDCs Reveals Presence of Glycolytic Reserve

(A) *Schematic of study design.* Glucose is transported into cells via glucose transporter 1 (GLUT1), and is metabolized by glycolysis to generate pyruvate, most of which is converted to lactate in proliferating cells. Iodoacetate (iodo) inhibits the glycolytic enzyme, glyceraldehyde-3-phosphate dehydrogenase (GAPDH). Pyruvate enters cells via the mono-carboxylate transporter (MCT) and is metabolized to lactate or acetyl-CoA by the pyruvate dehydrogenase complex (PDH), which is inhibited by HIF-1α. Pyruvate fuels oxidative phosphorylation (OxPhos) NRV, which is inhibited by oligomycin (oligo). **(B)** *Representative respirometry data* from cardiosphere-derived cells (CDCs) cultured in serum and glucose-containing medium. Inhibitors of the mitochondrial electron transport chain

(oligo, rotenone, antimycin A) suppressed oxygen consumption rate (OCR) and led to compensatory increase in glycolysis (extracellular acidification rate [ECAR]), indicated by **blue arrowheads**. FCCP, a protonophore that uncouples OxPhos, was used to quantify OxPhos capacity. Data is presented as mean ± SEM; n = 6. Significance was determined by 1-way analysis of variance (ANOVA)followed by Tukey's post-hoc test. **(C)** *Restriction of metabolic program* in CDCs to OxPhos (pyruvate), anaerobic glycolysis (DMOG), or aerobic glycolysis (control) reveals highest OxPhos capacity in pyruvate medium. ECAR was similar during anaerobic glycolysis and following inhibition of OxPhos by oligo for 24 h, during aerobic glycolysis. Data is presented as mean ±SEM; n = 6. Significance was determined by 1-way ANOVA followed by Tukey's post-hoc test. **(D)** *Oligo-sensitive ATP.* OxPhos inhibition for 30 to 45 min led to reduction in cellular ATP of 15% in glucose medium, 100% in pyruvate medium, and 0% in DMOG medium. Statistical significance is presented for total ATP levels (compared with control) and calculated using the unpaired Student *t* test. **(E)** *OxPhos inhibition* by oligo led to an increase in glucose (^{18}FDG) uptake and lactate generation in glucose medium. Iodo treatment significantly suppressed both glucose uptake and lactate generation, whereas HIF-1α stabilization by DMOG significantly increased glucose uptake and lactate generation by CDCs. The Student *t* test was used to determine significance. **(F)** *Mitochondrial membrane potential.* $\Delta\Psi_m$ is maintained following inhibition of OxPhos for 24 h during aerobic glycolysis (control) and anaerobic glycolysis (DMOG). Oligo induces $\Delta\Psi_m$ depolarization within 3 h in pyruvate medium. The Student *t* test was used to determine significance. **(G)** *Cell proliferation assay.* CDC proliferation continues, but at a reduced rate following oligo treatment during aerobic glycolysis. Cell proliferation ceases on days 2 to 3 in pyruvate medium and oligo leads to cell death within 1 day in pyruvate medium. CDCs proliferate during anaerobic glycolysis (DMOG), but at a reduced rate when compared with aerobic glycolysis (control). Oligo treatment has no effect on proliferation during anaerobic glycolysis. A 2-way ANOVA with repeated measure was used to evaluate differences between groups over time. **(H)** *Time course of Akt and AMPK activation following OxPhosinhibition* by oligo during aerobic glycolysis, anaerobic glycolysis, and OxPhos. Akt activationat 1 h following oligo treatment during aerobic glycolysis (control) is associated with reduction in AMPK phosphorylation, indicating reduction of energetic stress. Akt dephosphorylation and persistent AMPK activation is observed following inhibition of OxPhos in pyruvate medium. Oligo had little effect on AMPK and Akt signaling during anaerobic glycolysis (DMOG); (n = 3 for each time point. Results are presented as mean ± SD; n = 6 in each run; each experiment was repeated 3 times unless otherwise specified. **p < 0.01; ***p < 0.001. n.s. = nonsignificant.

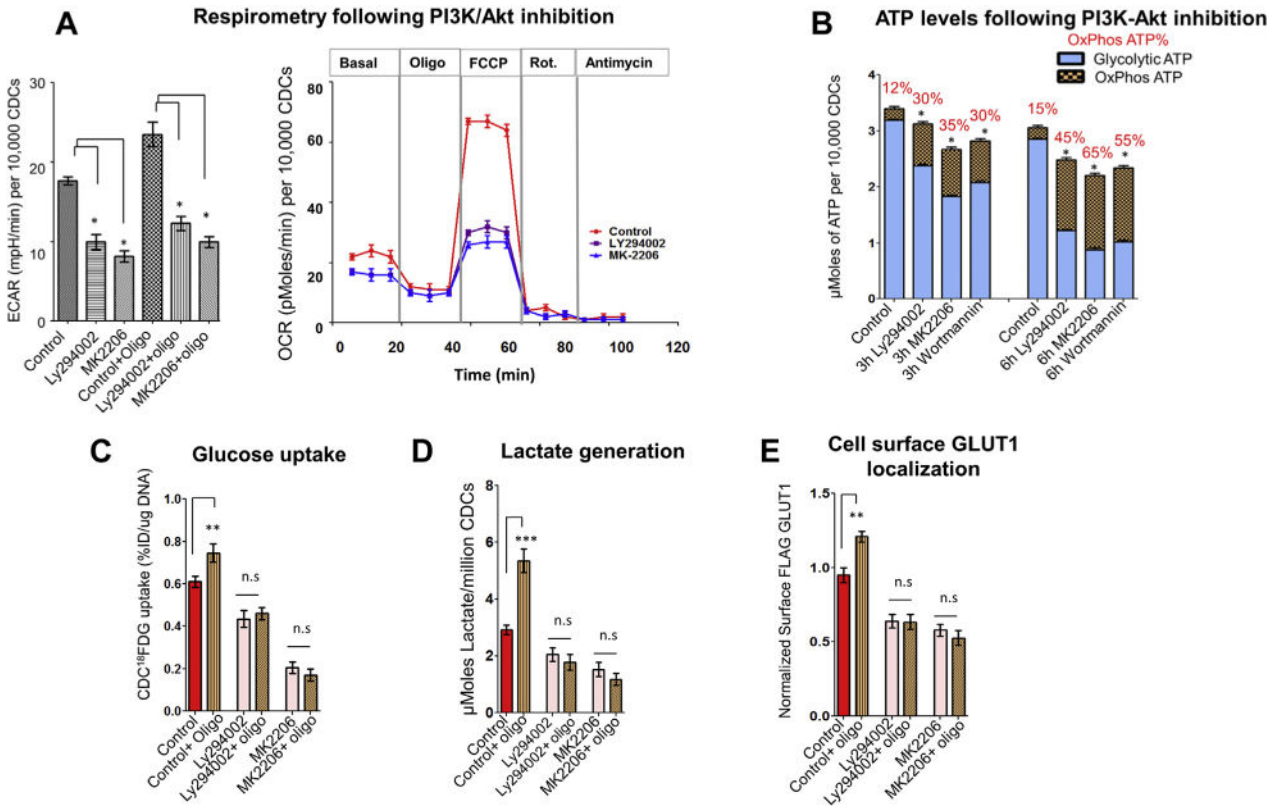

FIGURE 2. PI3K/AKT Signaling Is Required for Maintenance of Glycolytic Reserve

(A) PI3K-Akt inhibition reduced OxPhos capacity and glycolysis. ECAR data is presented as mean ± SEM; n = 4. The Student *t* test was used to assess effect of Akt inhibition on ECAR. One-way ANOVA with Tukey's post-hoc test was used to determine significance in OCR data. **(B)** PI3K/Akt inhibition reduced cellular ATP levels and ATP generation by glycolysis, but increased the contribution OxPhos to ATP generation. Data is presented as mean ± SD; n = 6; Student *t* test was used to determine significance. **(C and D)** Akt inhibition prevented compensatory increase in glucose (^{18}FDG) uptake and lactate generation following OxPhos inhibition by oligo in glucose medium. Effect of oligo on glucose uptake/lactate generation was examined using the Student *t* test. Data is presented as mean ± SD; n = 3; Student *t* test was used to determine significance. **(E)** Akt inhibition prevented increase in cell surface GLUT1 following OxPhos inhibition by oligo. Data is presented as mean ± SD; n = 6; Student *t* test was used to determine significance. Cells in the control condition in **C to E** were treated with vehicle (dimethyl sulfoxide). *p < 0.05; **p < 0.01. Abbreviations as in Figure 1.

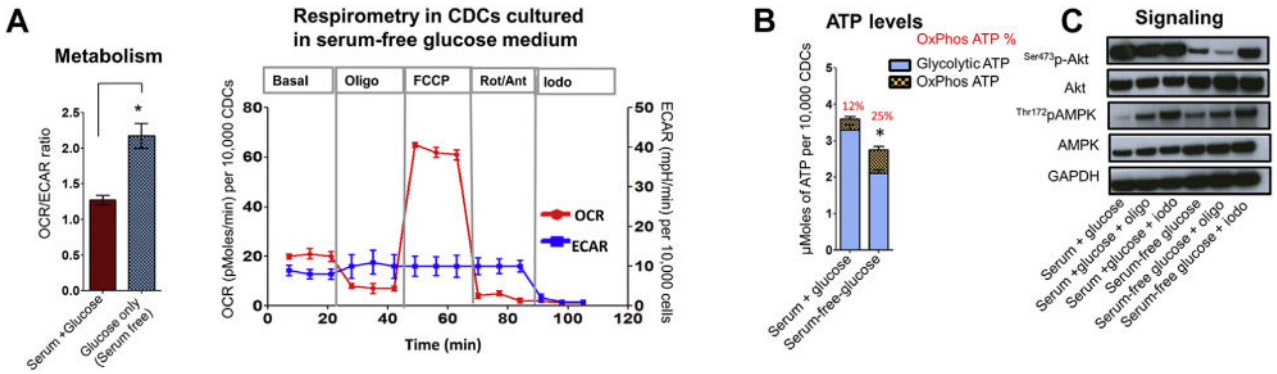

FIGURE 3. Serum Is Essential to Maintain Glycolysis and Glycolytic ATP

The effect of serum on energetics was assessed by serum withdrawal for 24 h prior to assays. **(A)** Respirometry. The OCR/ECAR ratio was increased following serum withdrawal, due to greater reduction of ECAR than OCR. Respirometry following serum withdrawal (24 h) led to significant reduction in ECAR and OCR. The Student t test was used to determine significance for OCR/ECAR data, and 1-way ANOVA with Tukey's post-hoc test was used to determine significance for OCR and ECAR data. **(B)** ATP. Serum withdrawal depressed cellular ATP levels, reduced glycolytic ATP, and increased the contribution of ATP generation by OxPhos. Statistical significance for total ATP levels was determined using the Student t test. Data is presented as mean ± SD; n = 6. **(C)** Signaling. Serum withdrawal leads to Akt dephosphorylation and AMPK activation. Glycolytic inhibition using iodo leads to AMPK activation in both serum and serum-free conditions; n = 3. *p < 0.05. Abbreviations as in Figure 1.

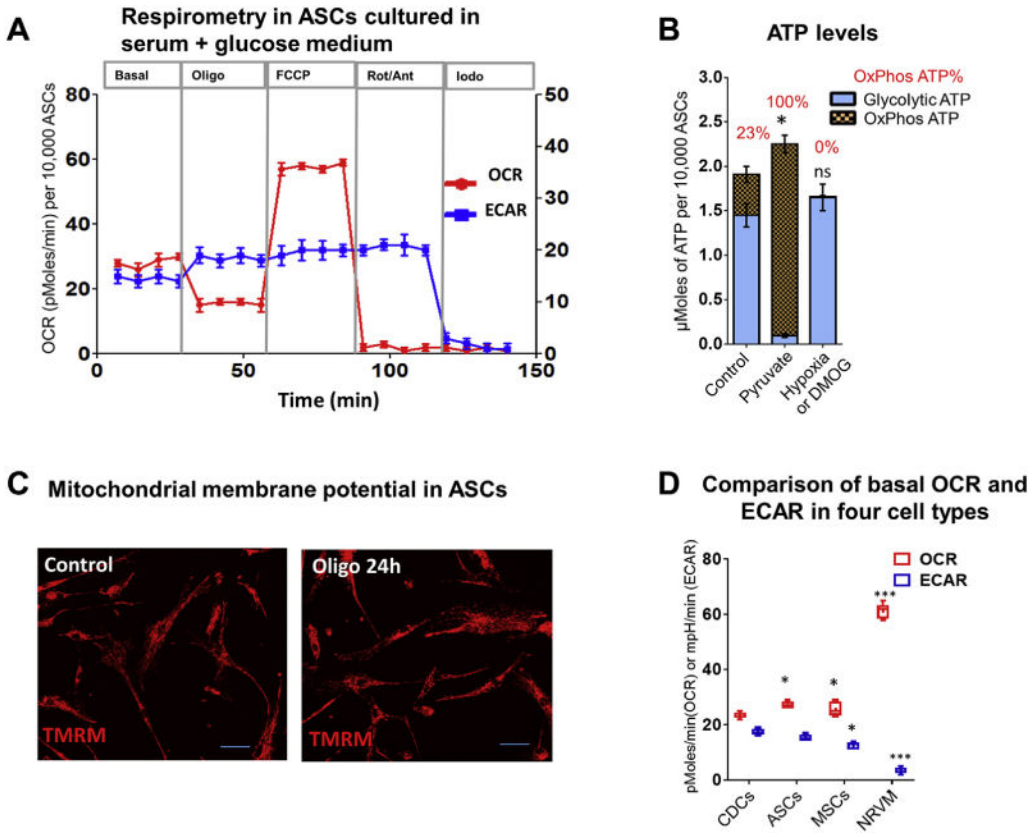

FIGURE 4. Human ASCs Demonstrate Glycolytic Reserve

(A) Respirometry. Adherent human ASCs exhibit increase in glycolysis (ECAR) following inhibition of OxPhos by oligo. One-way ANOVA with Tukey's post-hoc test was used to determine significance. **(B)** ATP. Metabolic program restriction to aerobic glycolysis (glucose), OxPhos (pyruvate), or anaerobic glycolysis (DMOG) reveals that OxPhos contributes to ~23% of cellular ATP in adherent ASCs, in the presence of serum and glucose. Replacement of glucose by pyruvate abolished ATP generation by glycolysis, whereas DMOG abolished ATP generation by OxPhos. Total ATP levels in ASCs cultured in the presence of pyruvate or DMOG/hypoxia were compared individually to total ATP levels in untreated cells (control) using the Student t test. **(C)** Glycolytic reserve. Inhibition of mitochondrial ATP synthesis in human adipocyte stromal cells (hASCs) by oligo (for 24 h) does not lead to $\Delta\Psi_m$ depolarization. Viability is preserved following OxPhos inhibition, confirming the presence of glycolytic reserve in hASCs. **Calibration bar** represents 50 µm **(D)** Comparison of energetics in adipocyte stromal cells (ASCs), mesenchymal stem cells (MSCs), CDCs, and neonatal rat ventricular myocytes. A comparison of basal respiration in 4 cell types, namely CDCs, ASCs, MSCs, and neonatal rat ventricular myocytes (NRVMs), revealed the highest OCR (OxPhos) and lowest ECAR (glycolysis) in NRVMs. Statistical significance was assessed using 1-way ANOVA followed by Tukey's post hoc test. Results are presented as mean ± SD with n = 6; each experiment was repeated 3 times. *$p < 0.05$. Abbreviations as in Figure 1.

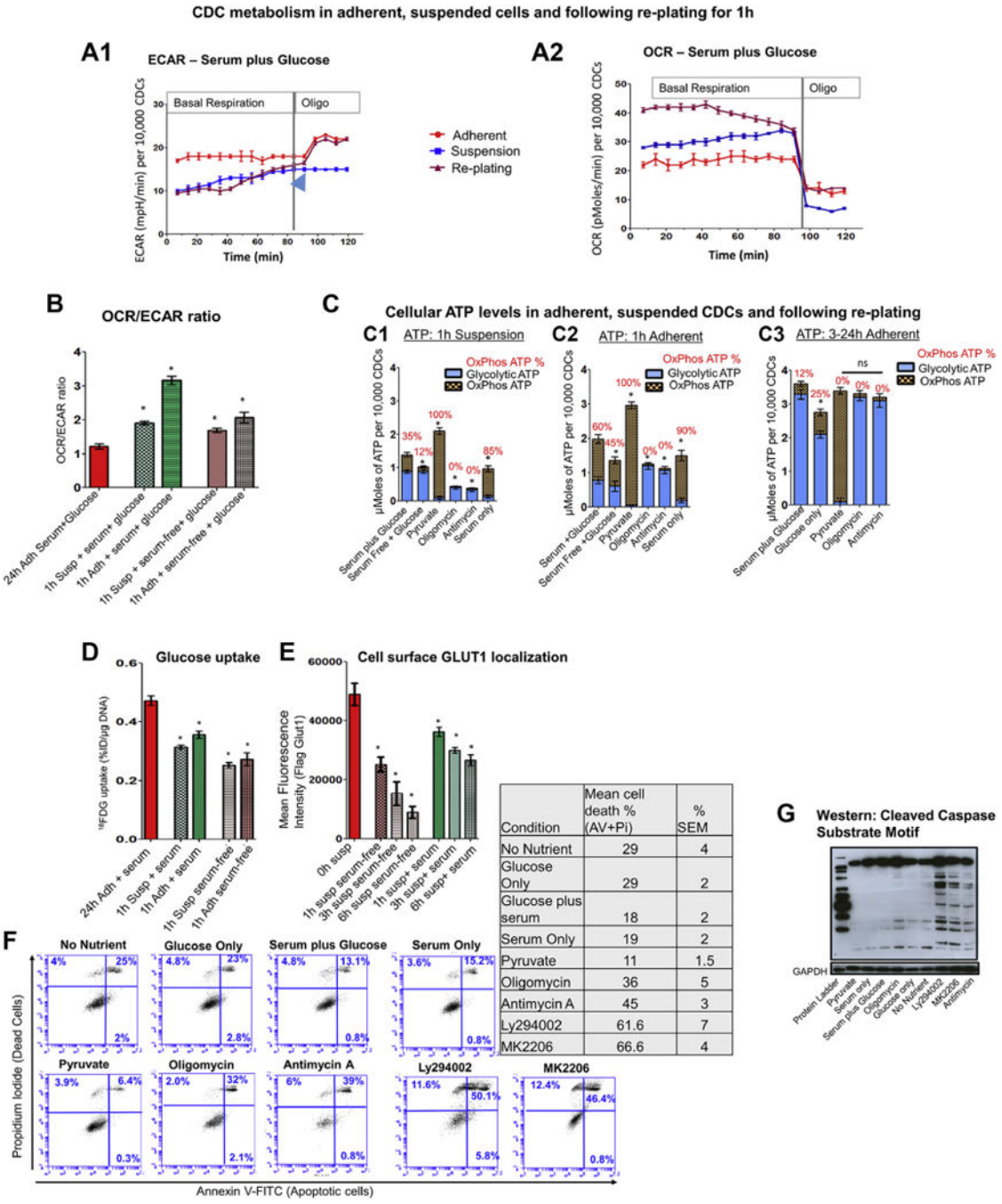

Condition	Mean cell death % (AV+Pi)	% SEM
No Nutrient	29	4
Glucose Only	29	2
Glucose plus serum	18	2
Serum Only	19	2
Pyruvate	11	1.5
Oligomycin	36	5
Antimycin A	45	3
Ly294002	61.6	7
MK2206	66.6	4

FIGURE 5. Cell Suspension Leads to Energetic Stress Due to Nutrient Limitation

(A1 and A2) Live respirometry in 24-h adherent, suspended, and replated CDCs. Adherent cells have higher glycolysis (ECAR) than suspended cells and re-plated cells. Cells in suspension and immediately following replating have higher OxPhos than cells adherent for 24 h. ECAR is restored within 60 to 90 min following replating. Cells in suspension do not exhibit increase in ECAR following oligo treatment, indicating a loss of glycolytic reserve **(blue arrowhead)**. Data is presented as mean ± SEM with n = 4. Two-way repeated ANOVA followed by Tukey's post-hoc test was used to compare respirometry data in the 3

groups. **(B)** OCR/ECAR ratio. Cell suspension and early replating are associated with significant increase in the OCR/ECAR ratio, due to a greater increase in OCR than ECAR when compared with cells adherent for 24 h. The Student t test was used to compare each condition, with results from 24-h adherent cells cultured in the presence of serum/glucose-containing medium (control). **(C)** Energetics. Suspension **(C1)** leads to a reduction in cellular ATP levels and increase in ATP generation by OxPhos, when compared with cells adherent for 3 to 24 h **(C3)**. Replacing glucose with pyruvate results in the highest ATP levels in suspended cells and early during early replating **(C2)**, but ATP levels are still lower than cells adherent for 3 to 24h **(C3)**. Cells fail to increase glycolytic ATP following inhibition of OxPhos by oligo in suspension, indicating loss of glycolytic reserve. Early replating **(C2)** increases ATP generation by OxPhos, but cellular ATP levels are lower than in cells adherent for 3 to 24 h. Statistical comparison for total ATP levels were performed using the Student t test. **(D)** Glucose (^{18}FDG) uptake. Cells in suspension and following replating demonstrate lower glucose uptake than cells adherent for 24 h. Statistical comparison was performed with glucose uptake by CDCs adherent for 24 h, using the Student t test. **(E)** Cell surface GLUT1 localization. Cell surface GLUT1 localization is significantly reduced within 1 h of suspension. Longer periods of suspension (3 to 6 h) leads to a progressive reduction of cell surface GLUT1 localization. GLUT1 levels were measured immediately following trypsinization, which is indicated as the 0-h time point, to control for the effect of trypsinization/cell harvesting on cell surface expression of GLUT1. Statistical comparison was performed with cell surface FLAG-GLUT1 at 0 h suspension using the Student t test. **(F)** Flow cytometry using Annexin V and PI. Replacing glucose by pyruvate or serum in cell suspensions reduces cell death at 1 h of suspension. In contrast, OxPhos inhibition by oligo, antimycin A, or inhibition of PI3K-Akt signaling markedly increased cell death in suspension (n = 3; each experiment was repeated twice). **(G)** Western blot. Caspage cleavage was used to confirm cell death in suspended cells in different treatment conditions; n = 2; 1 representative image is shown Results and presented as mean ± SD; n = 6. Each experiment was repeated 3 times unless otherwise specified. *$p < 0.05$. Abbreviations as in Figure 1.

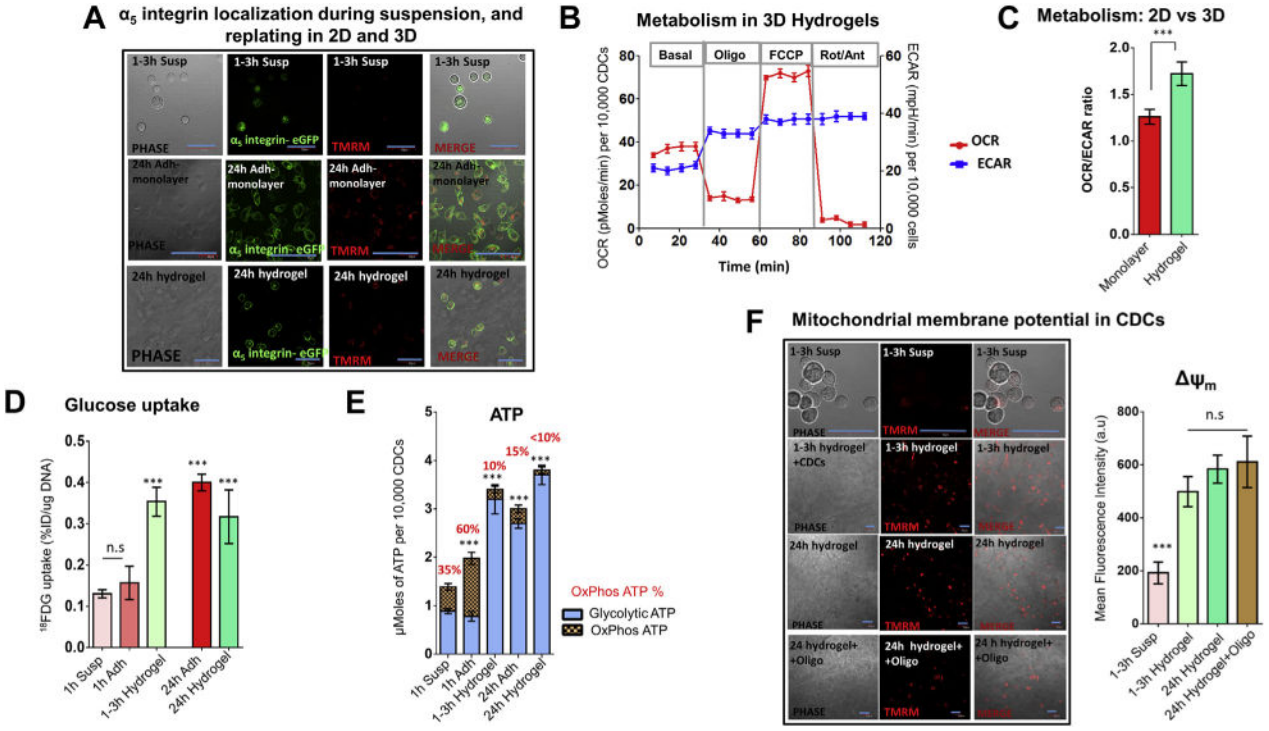

FIGURE 6. Energetics and Glycolytic Reserve Are Restored Following CDC Encapsulation in HA:Bl:Ser Hydrogels

(A) Integrin localization. Cell plating as 2D monolayers and encapsulation in HA:Bl:Ser hydrogels (but not cell suspension) leads to α_5-integrin localization in the cell membrane within 1 h, indicating activation of cell adhesion. Calibration bar in microscopy figures represents 50 μm. **(B and C)** Respirometry. Cell encapsulation in hydrogels leads to a rapid increase in OCR and ECAR. The OCR/ECAR ratio of cells encapsulated in hydrogels is higher than cells cultured as adherent monolayers. Statistical comparison was performed using 1-way ANOVA followed by Tukey's post-hoc test. **(D and E)** Glycolytic reserve. Glucose (^{18}FDG) uptake and glycolytic ATP generation are restored within 1 to 3 h of encapsulation in hydrogels. Statistical comparison was made using the Student t test with the 1-h suspension condition. **(F)** Mitochondrial membrane potential. ΔΨm, an indicator of cell viability, is maintained after inhibition of OxPhos by oligo (24 h), indicating presence of glycolytic reserve in cells encapsulated in hydrogels. Statistical comparison was made using the Student t test. against the 1- to 3-h suspension condition. Calibration bar represents 50 μm; n = 3. Hydrogels refers to HA:Bl:Ser hydrogels. Data is presented as mean ± SD. ***p < 0.001. Abbreviations as in Figure 1.

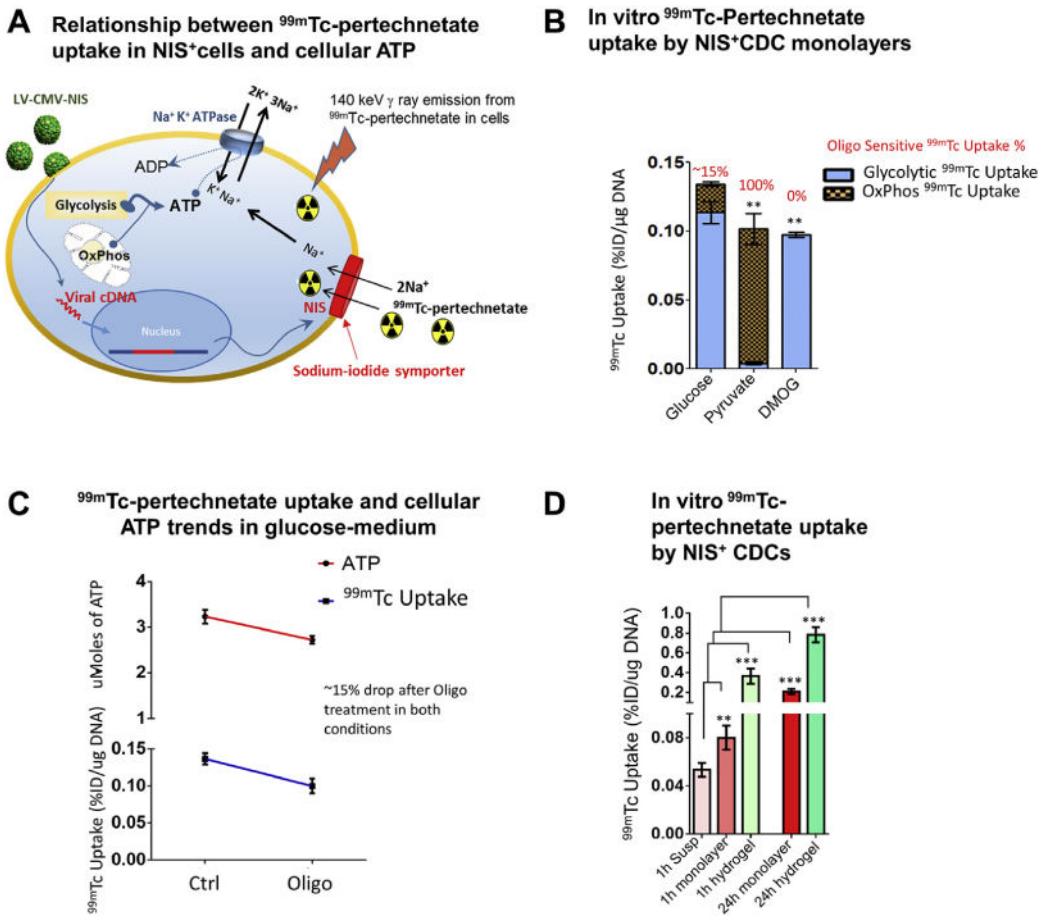

FIGURE 7. 99mTc-Pertechnetate Uptake Reflects In Vitro Cellular Energetics

(A) Schematic illustrating link between ^{99m}Tc-pertechnetate uptake and cellular ATP levels. Cells transduced with NIS (using lentivirus) take up ^{99m}Tc-pertechnetate, which permits cell tracking by single-photon emission computed tomography (SPECT). ^{99m}Tc-pertechnetate transport by NIS is dependent on the transmembrane Na^+ gradient, which is maintained by Na^+-K^+-ATPase. Because Na^+-K^+-ATPase activity is dependent on cellular ATP levels, cellular energetic state modulates ^{99m}Tc-pertechnetate uptake. **(B)** Oligo treatment led to a 15% reduction of ^{99m}Tc-pertechnetate uptake by NIS^+ cells. ^{99m}Tc-pertechnetate uptake by NIS^+ cells was abolished by oligo treatment when NIS^+ cells were cultured in pyruvate medium (OxPhos condition); oligo did not affect ^{99m}Tc-pertechnetate uptake when cells were cultured with DMOG (anaerobic glycolysis condition). Statistical comparison was performed between cells cultured in medium containing pyruvate or DMOG with cells cultured in glucose medium, using the Student t test. **(C)** Oligo treatment led to a 15% reduction in total cellular ATP (Figure 5C2) and ^{99m}Tc-pertechnetate uptake **(B)**, suggesting that ^{99m}Tc-pertechnetate uptake by NIS^+ cells reflects cellular ATP levels. **(D)** In vitro ^{99m}Tc-pertechnetate uptake was markedly reduced by suspension and restored by replating as monolayers or encapsulation in hydrogels. Statistical comparison of each condition was performed with 1-h suspension condition using the Student t test. Data is presented as mean ± SD; n = 6. **p < 0.01; ***p < 0.001. Abbreviations as in Figure 1.

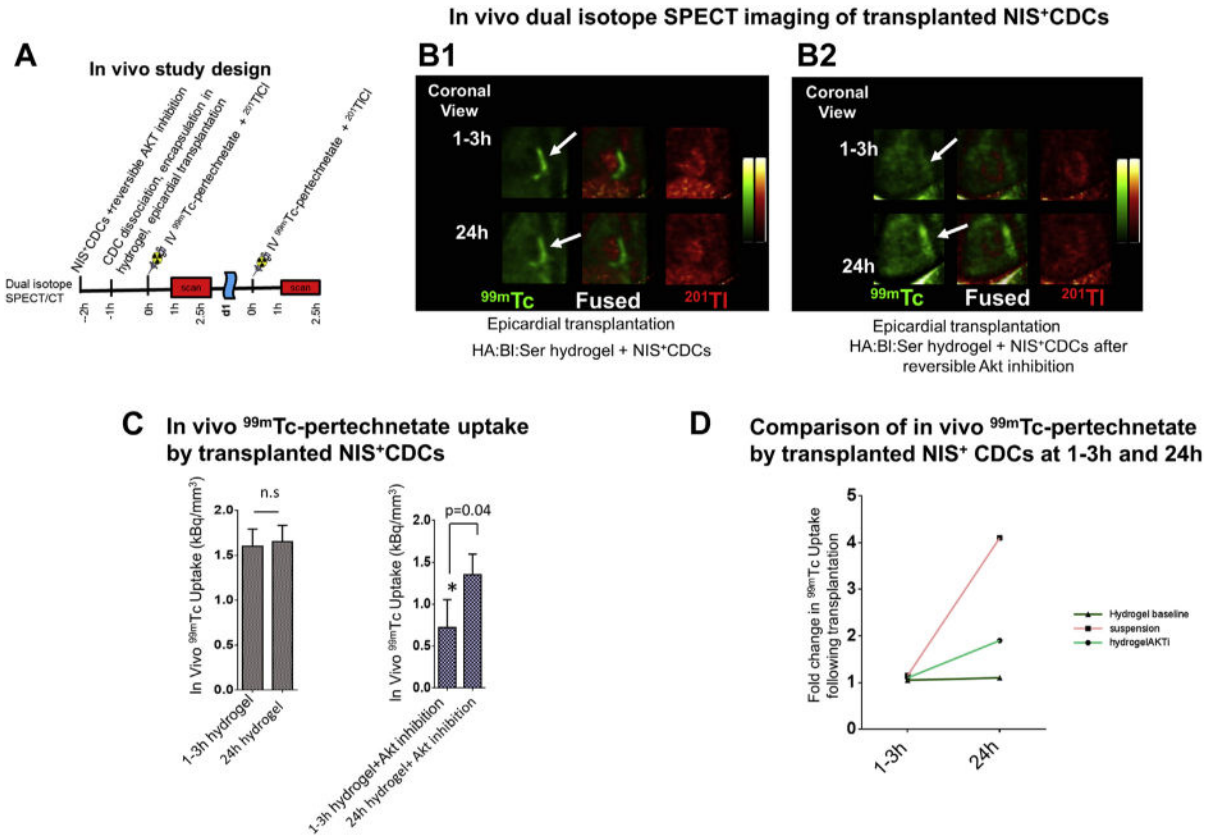

FIGURE 8. ^{99m}Tc-Pertechnetate Uptake Reflects In Vivo Cellular Energetics

(A) In vivo study design. In vivo dual isotope single-photon emission computed tomography/computed tomography (SPECT/CT) imaging was performed at 1 to 3 h and 24 h following epicardial transplantation of NIS$^+$ CDCs encapsulated in hydrogels, following intravenous injection of ^{99m}Tc-pertechnetate to track NIS$^+$ CDCs and ^{201}Tl-Cl to visualize myocardium. NIS$^+$ CDCs were treated with a reversible Akt inhibitor for 1 h prior to washout, dissociation, and encapsulation in hydrogels to demonstrate that reduction of cellular ATP levels leads to down-regulation of in vivo ^{99m}Tc-pertechnetate uptake by transplanted NIS$^+$ CDCs. **(B)** In vivo dual isotope SPECT/CT imaging. Representative coronal images of in vivo ^{99m}Tc-pertechnectate uptake (by NIS$^+$ CDCs) at 1 to 3 h and 24 h after epicardial transplantation of NIS$^+$ CDCs in noninfarcted rat myocardium. ^{99m}Tc-pertechnectate uptake by transplanted cells is represented in **green** and ^{201}Tl uptake by myocardium is represented in **red**. Encapsulation in hydrogels results in high ^{99m}Tc-pertechnectate uptake at 1 to 3 h following transplantation/encapsulation **(B1)**; reversible Akt inhibition resulted in lower ^{99m}Tc-pertechnectate uptake at 1 to 3 h post-transplantation when compared with 24 h **(B2). White arrows** indicate transplantation site. **(C)** Summary of in vivo ^{99m}Tc-pertechnectate uptake at 1 to 3 h and 24 h following encapsulation in hydrogels and reversible Akt inhibition. Encapsulation in hydrogels led to similar ^{99m}Tc-pertechnectate uptake at 1 to 3 h and 24 h post-transplantation. In contrast, reversible Akt inhibition in CDCs prior to transplantation led to significantly lower ^{99m}Tc-pertechnectate uptake at 1 to 3 h post-transplantation, when compared with 24 h. Statistical significance was determined using the Mann-Whitney U test. Data is presented as mean ± SD; n = 4. **(D)**

Figure illustrating trends for in vivo ^{99m}Tc-pertechnetate by transplanted NIS^{+} CDCs at 1 to 3 h and 24 h following intramyocardial transplantation of suspended NIS^{+} CDCs (historic data [3]), and following epicardial transplantation of NIS^{+} CDCs encapsulated in hydrogels with/without Akt inhibition **(C).** Cell suspension and Akt inhibition, which result in energetic stress, were associated with lower ^{99m}Tc-pertechnetate uptake at 1 to 3 h when compared to the 24-h time point, whereas hydrogel encapsulation alone resulted in similar uptake at these 2 time points. Abbreviations as in Figure 1.

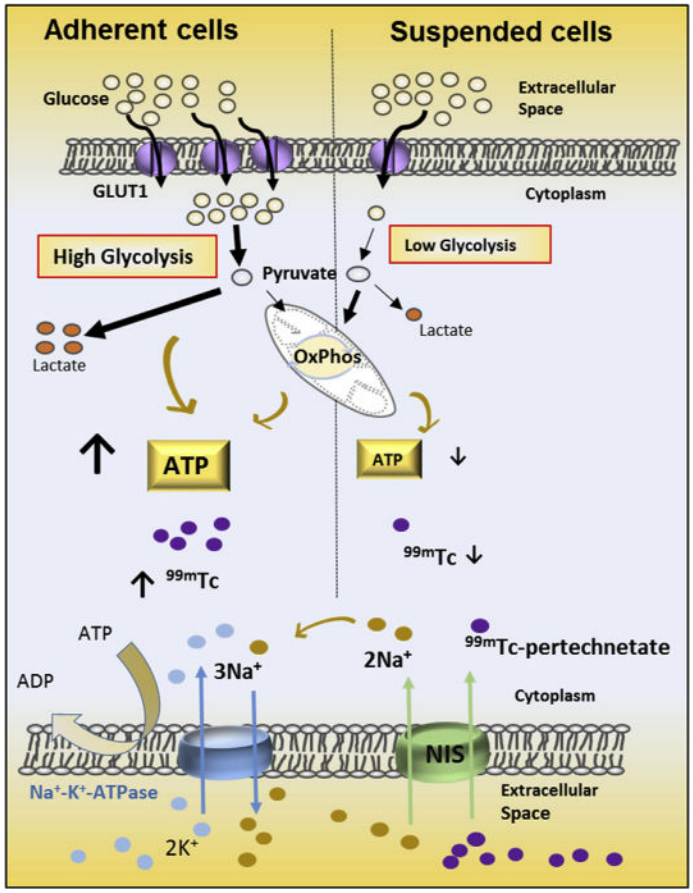

FIGURE 9. Cell Adhesion Status Influences Cellular Energetic State and ^{99m}TC-Pertechnetate Uptake

Schematic illustrating the relationship between energetics and ^{99m}Tc-pertechnetate uptake in adherent and suspended cells. Glycolysis is the main ATP-generating metabolic pathway in proliferating cells. Cell dissociation/suspension leads to reduced surface expression of GLUT1, reduced glucose uptake and glycolytic flux with consequent reduction in cellular ATP levels. NIS expression permits cellular transport of ^{99m}Tc-pertechnectate, which is coupled to Na^+-K^+-ATPase activity, and modulated by cellular ATP levels. Suspended cells have down-regulation of glycolysis, lower cellular ATP levels, and lower ^{99m}Tc-pertechnectate uptake, when compared with adherent cells. Abbreviations as in Figure 1.